# Stripes and honeycomb lattice of quantized vortices in rotating two-component Bose-Einstein condensates

Kenichi Kasamatsu and Kouhei Sakashita
*Department of Physics, Kindai University, Higashi-Osaka, Osaka 577-8502, Japan*

(Received 18 March 2018; published 29 May 2018)

We study numerically the structure of a vortex lattice in rotating two-component Bose-Einstein condensates with equal atomic masses and equal intra- and intercomponent coupling strengths. The numerical simulations of the Gross-Pitaevskii equation show that the quantized vortices in this situation form lattice configuration accompanying vortex stripes, honeycomb lattices, and their complexes. This is a result of the degeneracy of the system for the SU(2) symmetric operation, which causes a continuous transformation between the above structures. In terms of the pseudospin representation, the complex lattice structures are identified as a hexagonal lattice of doubly winding half skyrmions.

DOI: 10.1103/PhysRevA.97.053622

## I. INTRODUCTION

Quantized vortices are the basic constituents of superfluid hydrodynamics, having a definite quantized circulation. When a superfluid is subject to an external rotation, the superfluid forms a lattice of quantized vortices, creating rigid-body rotation. In usual superfluids with the scaler order parameter, the vortices form a triangular Abrikosov lattice [1]. Conversely, for unusual superfluids characterized by, e.g., multiple order parameters, a rich variety of vortex lattice structures can emerge because the vortices in such superfluids have a complex core structure and there are multiple scales of interactions between them [2].

Multicomponent superfluids have been realized by cold atomic Bose-Einstein condensates (BECs) [3] and the vortex structures have been studied very well [4]. The observation of vortex lattices in rotating multicomponent BECs has been reported in Ref. [5]. It has been known that rotating two-component BECs have a rich vortex lattice structure, which is particularly dependent on the intercomponent interaction [6–17]. In cold-atom experiments, the intercomponent interaction may be considered as a tunable parameter [18,19]. In the absence of intercomponent interaction, the two condensates behave independently and the vortex lattice then forms a triangular lattice, as in conventional scalar condensates. When the intercomponent coupling is positively increased, the repulsive interaction between two components displaces the lattice locations, thereby decreasing the overlapping of the condensate densities. Then the triangular lattice deforms into an interlaced square lattice. A further increase of intercomponent repulsion induces the phase separation of the two components. Subsequently, the periodic structure of the vortex lattice transforms into interwoven vortex sheets [7,20]. Alternatively, one can consider the attractive force between two components by decreasing the intercomponent coupling to a negative value. Then the location of the vortices is locked to the same position [6,8,13].

However, the phase diagram of the vortex lattice structures has not been fully understood. It is noticeable that, when the all intercomponent and intracomponent couplings are equivalent, with the Hamiltonian having an exact SU(2) symmetry, one peculiar structure of the vortex lattice appears, namely, honeycomb and double-core lattices. This has been observed in numerical simulations of the coupled Gross-Pitaevskii (GP) equations [7,10] and Monte Carlo simulation of similar models [21]. Conversely, the theoretical analysis based on the lowest Landau level approximation has predicted that the vortex stripe, the alternating rows of vortices in each component, is the stable structure [6]. So far, there is no theoretical interpretation of the problem of what true stable structures in this situation are. Therefore, it is necessary to clarify this problem to understand the complete phase diagram of vortex lattices in rotating two-component BECs. In this paper we demonstrate that both the stripe and the honeycomb lattice are true stable structures of fast rotating two-component BECs with an SU(2) symmetry. We find that these structures are connected through the global SU(2) rotation and identical to a lattice of doubly winding half skyrmions in the pseudospin picture.

This paper is organized as follows. After introducing the theoretical formulation in Sec. II A, we provide some numerical evidence of the vortex lattice structures in Sec. II B. Following this numerical observation, in Sec. III we attempt to explain the mechanism of why the honeycomb lattice structure appears in two-component BECs.

## II. VORTEX STATES IN ROTATING TWO-COMPONENT BECs

After introducing the theoretical formulation for describing the two-component BECs, we provide a brief account of the vortex lattice structures in this system through a numerical simulation of the GP equations.

 

### A. Coupled Gross-Pitaevskii equations

The equilibrium solutions of vortex states in rotating two-component BECs can be obtained by a minimization of the GP energy functional

$$E[\Psi_1,\Psi_2] = \int d\boldsymbol{r} \sum_{i=1,2} \Psi_i^*(\hat{h}_i - \Omega \hat{L}_z)\Psi_i + E_{\rm int}, \quad (1)$$

$$E_{\rm int} = \int d\boldsymbol{r}\Big(\frac{g_1}{2}|\Psi_1|^4 + \frac{g_2}{2}|\Psi_2|^4 + g_{12}|\Psi_1|^2|\Psi_2|^2\Big) \quad (2)$$

in a rotating frame with a rotation frequency of $\Omega = \Omega\hat{\boldsymbol{z}}$. Here $\hat{h}_i = -\hbar^2\nabla^2/2m_i + V^i_{\rm ext}(\boldsymbol{r})$ is a single-particle Hamiltonian, $m_i$ is the atomic mass of the $i$th component ($i = 1,2$), and the interaction strengths are given as $g_i = 4\pi\hbar^2 a_i/m_i$ and $g_{12} = 2\pi\hbar^2 a_{12}/m_{12}$ with the intra- and intercomponent $s$-wave scattering lengths $a_i$ and $a_{12}$ and the reduced mass $m_{12}^{-1} = m_1^{-1} + m_2^{-1}$. To discuss the lattice structure, it is enough to confine ourselves to analyzing the equation in a two-dimensional (2D) $x$-$y$ plane. To scale the equation, we introduce the length and time scales of the trapping potential $V^i_{\rm ext} = m_i\omega_i^2 r^2/2$ as $a_{\rm ho} = \sqrt{\hbar/2m_{12}\bar{\omega}}$ and $\bar{\omega}^{-1}$, respectively, with $\bar{\omega} = (\omega_1 + \omega_2)/2$. In a 2D system, the wave function is normalized by the particle number $N_i^{\rm 2D}$ ($i = 1,2$) in two dimensions as $\Psi_i \to \sqrt{N_i^{\rm 2D}}\Psi_i/a_{\rm ho}$. We then obtain the dimensionless GP equation

$$\Big[-\frac{m_{12}}{m_1}\nabla^2 + \tilde{V}_1 + C_{11}|\Psi_1|^2 + C_{12}|\Psi_2|^2 - \tilde{\Omega}L_z\Big]\Psi_1 = \mu_1\Psi_1, \quad (3)$$

$$\Big[-\frac{m_{12}}{m_2}\nabla^2 + \tilde{V}_2 + C_{22}|\Psi_2|^2 + C_{21}|\Psi_1|^2 - \tilde{\Omega}L_z\Big]\Psi_2 = \mu_2\Psi_2. \quad (4)$$

Here the rotation frequency is $\tilde{\Omega} = \Omega/\bar{\omega}$ and the trapping potential is $\tilde{V}_i = \frac{1}{4}\frac{m_i}{m_{12}}\frac{\omega_i^2}{\bar{\omega}^2}(x^2 + y^2)$. The interatomic interactions for the intra- and intercomponent are written as

$$C_{ii} = 8\pi\frac{m_{12}}{m_i}N_i^{\rm 2D}a_i, \quad C_{ij} = 4\pi N_j^{\rm 2D}a_{12} \quad (i \neq j), \quad (5)$$

where the $s$-wave scattering length is confined to be positive. Given that the particle number of each component is conserved, the chemical potential $\mu_i$ is determined by a normalization of the wave function $\int dx\,dy|\Psi_i|^2 = 1$.

### B. Vortex lattice phase: Numerical study

Here we briefly mention the properties of vortex lattices in rotating two-component BECs. In this study our interest is focused on the vortex states when the Hamiltonian has an exact SU(2) symmetry. Thus, we confine ourselves to the parameters $m_1 = m_2 = m$, $\omega_1 = \omega_2 = \omega$, $N_1^{\rm 2D} = N_2^{\rm 2D} = N$, and $C_{11} = C_{22} = C > 0$. Setting $C = 4000$, we search the equilibrium solutions of Eqs. (3) and (4) by changing $\tilde{\Omega}$ as well as $\delta = C_{12}/C$ in the vicinity of unity.

Even for $\tilde{\Omega} = 0$ the equilibrium solutions of Eqs. (3) and (4) exhibit a rich variety of structures, depending on the various parameters of the system [4]. A salient feature is the occurrence of phase separation. In our parameter setting, the two components are miscible for $\delta < 1$ and immiscible for $\delta > 1$.

The properties of the vortex phases are also different for these two situations. In the miscible regime, the vortices form an interlaced triangular or square lattice depending on the ratio of the coupling strengths $\delta$ and the rotation frequency $\tilde{\Omega}$. The triangular lattice is a conventional lattice structure seen in rotating superfluids and type-II superconductors under a magnetic field, but the square lattice is an exotic structure in multicomponent superfluids. The transition of the lattice structure in two-component BECs has been discussed theoretically by using variational analysis based on the lowest Landau level expansion [6] and the argument based on the vortex-vortex interaction [12]. In the immiscible regime, the phase separation favors the formation of vortex sheets or rotating droplets when the condensates are subject to external rotation [20]. These behaviors can be understood through the ferromagnetic or antiferromagnetic nature of the interactions between coreless vortices [4]. Our focus is the vortex lattice structure at the boundary between the miscible and immiscible regimes. This situation is approximately realized in the experiments of two-component BECs with $^{87}$Rb atoms [22].

We first show the numerical results of the vortex lattice in two-component BECs around $\delta = 1$. Using the imaginary-time propagation of the time-dependent version of Eqs. (3) and (4), we calculate the equilibrium solutions. We confirm the sufficient convergence of certain quantities such as the total energy of the system. We conducted the simulations for several values of $\tilde{\Omega}$, $\delta$, and initial trial functions with the Gaussian form. Typical examples of the obtained structures are shown in Fig. 1. As mentioned, the clear square lattice [Fig. 1(a)] and vortex sheet structure [Fig. 1(c)] appear for $\delta \lesssim 1$ and $\delta \gtrsim 1$, respectively. For $\delta = 1$, the vortex lattice exhibits a more complicated form as shown in Fig. 1(b). For the $\Psi_2$ component, a clear structure of the honeycomb structure can be seen. For the $\Psi_1$ component, the two vortex cores are closely approached at the cells of the honeycomb created by the $\Psi_2$ vortices. Thus, this structure has been referred to as a double-core lattice [7]. This indicates that the symmetry of the solutions is spontaneously broken because the interdistance of the vortex core in each component is different, even for our symmetric parameter setting.

Throughout the numerical simulations starting from various initial conditions, we can observe various metastable configurations of the vortex lattices in addition to Fig. 1(b). The typical one is a stripe structure, where vortices in each component align rows alternately (like those shown in Fig. 2). The vortex stripe structure was predicted by Mueller and Ho as the stable lattice state for $\delta = 1$ [6]. However, the perfect periodicity of the ansatz cannot describe the honeycomb lattice characterized by different periodicities as shown in Fig. 1(b). In other cases, some defects remain in the honeycomb lattice, which decays very slowly during the imaginary-time propagation. For example, there appears a domain wall separating two configurations with a honeycomb lattice and a double-core lattice with different intervortex distances.

Next, in order to observe the stability of the honeycomb–double-core lattice, we start the imaginary-time propagation from the solution of Fig. 1(b) and change $\delta$ slightly from unity. We find that the honeycomb–double-core lattice is deformed

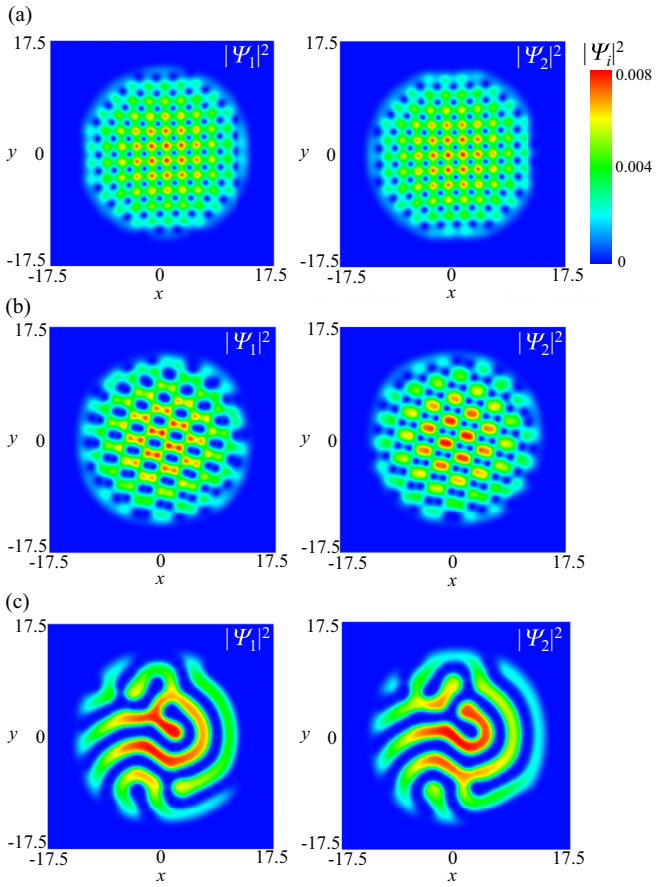


FIG. 1. Density profiles $|\Psi_1|^2$ (left) and $|\Psi_2|^2$ (right) of the equilibrium solutions of Eqs. (3) and (4) for $C = 4000$, $\tilde{\Omega} = 0.8$, and (a) $\delta = 0.9$, (b) $\delta = 1.0$, and (c) $\delta = 1.1$.

to the stripe structure, as shown in Fig. 2, for $|\delta - 1| \geqslant 0.005$. This result indicates that the lattice structure is consistent with the prediction of Ref. [6] except for $\delta = 1$. Therefore, the appearance of the honeycomb–double-core lattice is peculiar to the solution only for $\delta = 1$.

## III. VORTEX LATTICE STRUCTURE THROUGH SU(2) TRANSFORMATION

According to the numerical simulation, the vortex lattice structure is anomalous only for $\delta = 1$, where the coupling constants are equivalent as $g_1 = g_2 = g_{12}$. Then the two-component system in our case has an exact SU(2) symmetry. This is because the interaction energy of Eq. (2) can be simply written as $E_{\rm int} = (g/2)\int d\mathbf{r}\, n_{\rm T}^2$ with the total density $n_{\rm T} = |\Psi_1|^2 + |\Psi_2|^2$. Then the energy is invariant under the global SU(2) symmetric operation

$$\mathrm{SU}(2) = e^{-i\gamma\hat{\sigma}_z/2} e^{-i\beta\hat{\sigma}_y/2} e^{-i\alpha\hat{\sigma}_z/2} = \begin{pmatrix} \cos(\beta/2)e^{-i(\alpha+\gamma)/2} & -\sin(\beta/2)e^{i(\alpha-\gamma)/2} \\ \sin(\beta/2)e^{-i(\alpha-\gamma)/2} & \cos(\beta/2)e^{i(\alpha+\gamma)/2} \end{pmatrix}, \tag{6}$$

where $\boldsymbol{\sigma} = (\sigma_x, \sigma_y, \sigma_z)$ is the Pauli matrix and $(\alpha, \beta, \gamma)$ are the Euler angles. Here we see how the vortex lattice changes through the SU(2) transformation. Given that the rotation of

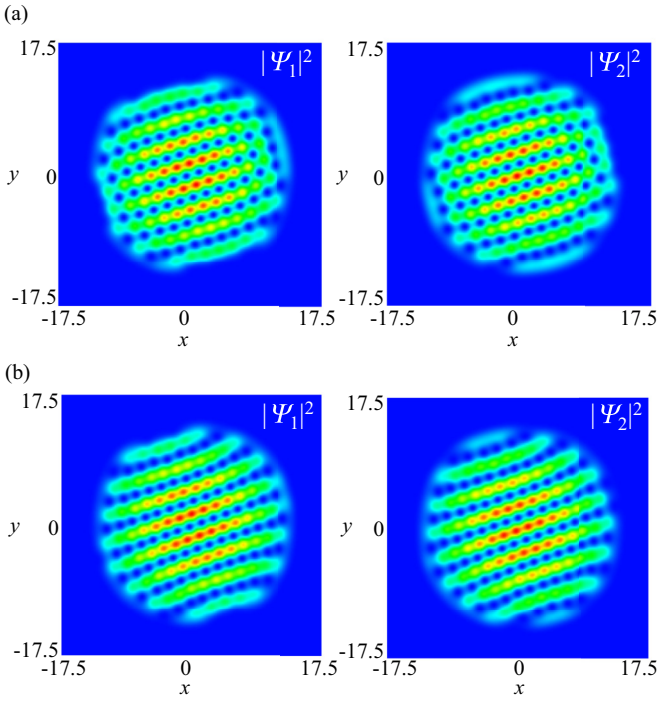


FIG. 2. Density profiles $|\Psi_1|^2$ (left) and $|\Psi_2|^2$ (right) of the equilibrium solutions of Eqs. (3) and (4) for $C = 4000$, $\tilde{\Omega} = 0.8$, and (a) $\delta = 0.995$ and (b) $\delta = 1.005$. The initial condition of the imaginary-time evolution corresponds to the solution of Fig. 1(b).

the angles $\alpha$ and $\gamma$ only changes the global phase of the wave function by a constant, this is not relevant to the lattice structure. Thus, the structural change of the vortex lattice may occur through the variation of $\beta$, which represents the rotation of the spin space around the $y$ axis.

The left panels of Fig. 3 show the change of the lattice structure through the rotation of $\beta$. Here we start from the solution of Fig. 1(b) as the state of $\beta = 0$. We can see that the stripe state and the honeycomb–double-core lattice are connected *continuously* by the $\pi/4$ rotation of $\beta$ as shown in Fig. 3(a). For $\beta = \pi/2$ the structure is similar to that in Fig. 1(b), but the pairs of the vortices forming double cores are exchanged with the nearest-neighbor ones. For $\beta = 3\pi/4$ the condensates form a nested structure consisting of lattices of vortex pairs as seen in Fig. 3(c), where the polarization of the pairs is almost perpendicular to the stripes at $\beta = \pi/4$. With further increasing $\beta$ to $\pi$, the structure of the $\Psi_1$ and $\Psi_2$ components is interchanged with that in Fig. 1(b) [Fig. 3(d)]. It is important to mention that these structures are degenerate with respect to the SU(2) transformation. Hence, one trial of the imaginary-time propagation of the GP equation selects one of the degenerate states. This is the reason why the numerical calculations yield many metastable configurations.

It is fruitful to see this structural transformation from the viewpoint of the pseudospin texture. The two-component BECs can be represented by a two-component spinor and the local pseudospin of the two-component system can be defined by $\boldsymbol{S} = \boldsymbol{\Psi}^\dagger \boldsymbol{\sigma} \boldsymbol{\Psi}/n_{\rm T}$ with $\boldsymbol{\Psi} = (\Psi_1, \Psi_2)^{\rm T}$ [4]. The right panels of Fig. 3 show the pseudospin profile of the corresponding state for each $\beta$. The spin points out of (into) the page at the vortex center of $\Psi_1$ ($\Psi_2$), around which the spin direction

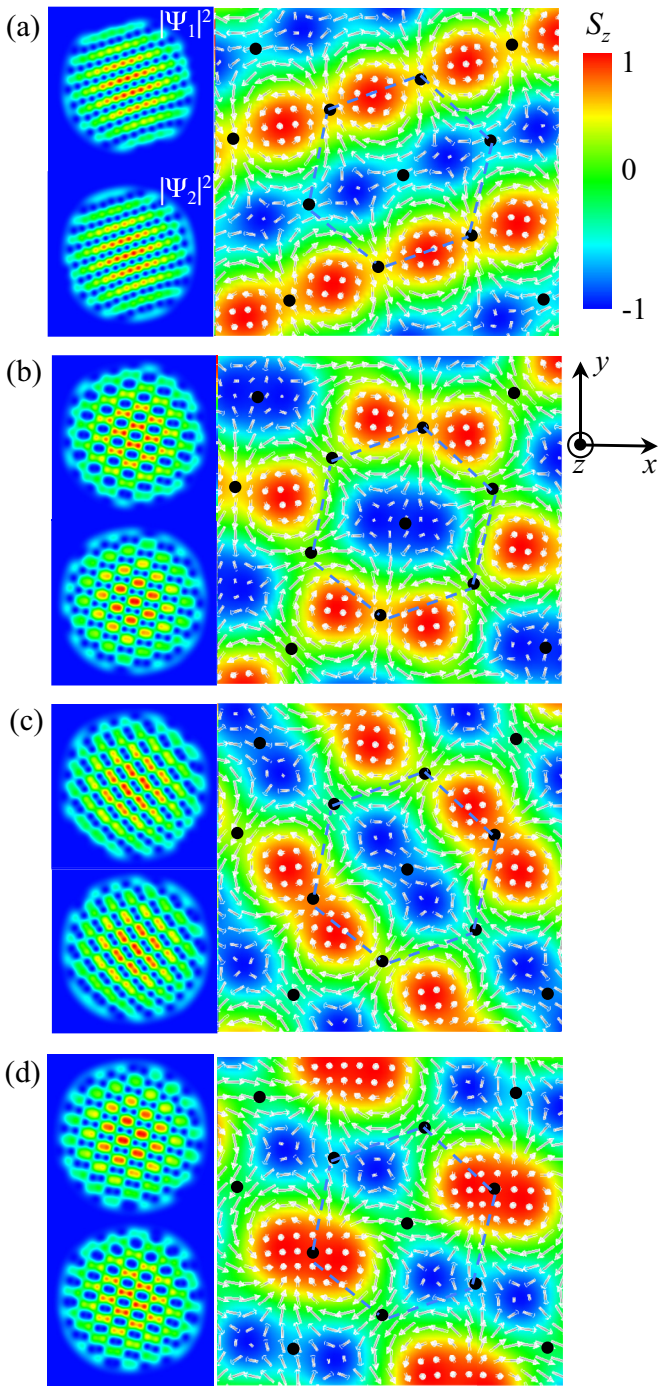


FIG. 3. The left panels show the density profiles $|\Psi_1|^2$ (top) and $|\Psi_2|^2$ (bottom) with the vortex lattice for $\delta = 1$ through the change of the Euler angle $\beta$ from that of Fig. 1(b). The values of $\beta$ are (a) $\pi/4$, (b) $\pi/2$, (c) $3\pi/4$, and (d) $\pi$. The profiles are plotted in the region $-17.5 \leqslant x, y \leqslant 17.5$. The right panels show the distribution of the spin $\boldsymbol{S}(\boldsymbol{r})$ of the corresponding solution in the region $-2.5 \leqslant x, y \leqslant 2.5$. The magnitude of $S_z$ is shown by the color scale. The black dots represent the points where the topological charge $q(\boldsymbol{r})$ vanishes; see Fig. 4(b).

covers the northern hemisphere (southern hemisphere) of the spin space, e.g., $2\pi$ sr of the solid angle. This structure is known as the half skyrmion (meron). For the vortex stripe

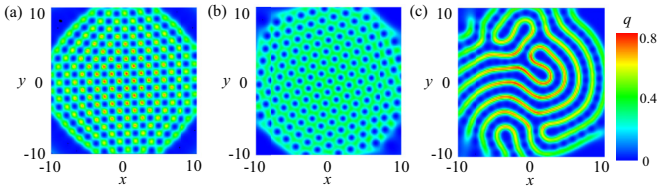


FIG. 4. Profile of the topological charge density for $\Omega = 0.8$ and (a) $\delta = 0.9$, (b) $\delta = 1.0$, and (c) $\delta = 1.1$, corresponding to the solution of Fig. 1. The topological charge is calculated within the Thomas-Fermi radius.

($\beta = \pi/4$), the pseudospin forms an alternative array of the half skyrmions with the spins at the center pointing up and down. Let us look at the structure in the hexagonal cell shown by the dashed line in Fig. 3(a). There are four cores of the skyrmions where the spins are pointing into or out of the page. By globally rotating the spins by $\pi/4$ around the $y$ axis, there appears a region with $S_z \sim 1$ at the center of the hexagon, around which the directions of the spins cover the southern hemisphere twice [Fig. 3(b)]. Thus, this structure corresponds to the doubly winding half skyrmion. Mueller showed that the doubly winding half skyrmion and the four half skyrmions are connected through the rotation of the angle $\beta$ [23]. This doubly winding half skyrmion is surrounded by the six half skyrmions. These composites can be seen as the honeycomb and double-core lattices in the density profile. With increasing $\beta$ further, the doubly winding half skyrmion again splits into two half skyrmions into the direction perpendicular to the original stripe [Fig. 3(c)]. For $\beta = \pi$ [Fig. 3(d)] the doubly winding half skyrmion with $S_z = +1$ at the core appears next to the noticeable hexagon.

We also calculate the profile of the topological charge density defined by

$$q(\boldsymbol{r}) = \frac{1}{4\pi} \boldsymbol{S} \cdot \left( \frac{\partial \boldsymbol{S}}{\partial x} \times \frac{\partial \boldsymbol{S}}{\partial y} \right). \tag{7}$$

In Fig. 4 we plot the profile of the topological charge corresponding to the solutions of Fig. 1. We can see the clear structural change between the typical lattice structures. The stripe and honeycomb–double-core lattice correspond to the hexagonal lattice of the "holes" of the topological charge $q(\boldsymbol{r})$ as shown in Fig. 4(b), which is clearly distinguished from the square lattice for $\delta \lesssim 1$ [Fig. 4(a)] and the vortex sheets for $\delta \gtrsim 1$ [Fig. 4(c)]. The hole of $q(\boldsymbol{r})$ is a clear signature of the doubly winding half skyrmion [23], where the topological charge is distributed around the skyrmion core. The magnitude of $q(\boldsymbol{r})$ in Fig. 4(b) is almost half of that in Figs. 4(a) and 4(c).

Note that an exact SU(2) symmetry operation is impossible in our case because each particle number of the two-component BEC must be conserved. The change of $\beta$ causes a population transfer between the two components. However, the approximate SU(2) operation is possible because of the presence of the vortices, which disturbs the spatial phase distribution of the condensate wave function. This can be seen by the fact that the norm of the wave function after the SU(2) transformation

$\mathbf{\Psi} \to \mathbf{\Psi}'$ can be written as

$$\int d\mathbf{r}|\Psi_i'|^2 = \int d\mathbf{r}\Big[\cos^2\frac{\beta}{2}|\Psi_i|^2 + \sin^2\frac{\beta}{2}|\Psi_j|^2 \mp 2\cos\frac{\beta}{2}\sin\frac{\beta}{2}|\Psi_i||\Psi_j|\cos(\theta_2-\theta_1-\alpha)\Big]. \tag{8}$$

If the third term of the right-hand side vanishes, the SU(2) operation does not change each of the particle numbers. Now the relative phase $\theta_2 - \theta_1$ is not physically relevant in our case because there is not Josephson-like coupling between the two components [14,17,24,25]. However, the presence of vortices yields the periodic spatial variation of $\theta_2 - \theta_1$ such that the spatial integral of the third term can vanish approximately. Thus, the spin rotation of the angle $\beta$ can be effectively achieved. This is the reason why the vortex lattice structure is fragile in this SU(2) symmetrical case. The presence of many vortices opens the door for the structural change associated with the SU(2) degeneracy.

## IV. SUMMARY AND DISCUSSION

In this paper we discussed the vortex lattice structure in rotating two-component BECs with equal intra- and inter-component interaction strengths. The Hamiltonian is rendered invariant under the SU(2) operation. The resulting degeneracy brings forth a rich variety of configurations of the vortex lattices, where the honeycomb–double-core lattices and stripes can coexist. These structures can be connected by a continuous global SU(2) transformation. Thus, the prediction by Mueller and Ho [6] is valid even at this SU(2) symmetric point.

In the experiments, the approximate SU(2) symmetry holds for the two-component BECs of $^{87}$Rb with the hyperfine spins $|1,-1\rangle$ and $|2,1\rangle$. In the experiments, the authors observed that the vortex lattices are fragile in the early stages of the dynamics before demonstrating the order of the square structures. Although this represents the nonequilibrium situation, it might be partly due to the degeneracy of the system. It is interesting to observe the stripe or honeycomb–double-core structures by tuning the coupling strengths to satisfy the SU(2) symmetry exactly. In other words, the observation of the fragile structure could be a consequence of the SU(2) symmetry. In order to see a rigid honeycomb–double-core structure, further fine-tuning of the parameters, such as the $s$-wave scattering lengths [18,19], is necessary to realize the scenario. In addition, our argument would be useful for discussing the vortex lattices in spinor BECs characterized by high-symmetry groups.

## ACKNOWLEDGMENTS

This work was partly supported by KAKENHI from JSPS (Grant No. 26400371).

[1] E. B. Sonin, *Dynamics of Quantised Vortices in Superfluids* (Cambridge University Press, Cambridge, 2016).
[2] For example, O. V. Lounasmaa and E. Thuneberg, Vortices in rotating superfluid $^3$He, Proc. Natl. Acad. Sci. U.S.A. **96**, 7760 (1999).
[3] C. J. Pethick and H. Smith, *Bose-Einstein Condensation in Dilute Gases*, 2nd ed. (Cambridge University Press, New York, 2008).
[4] K. Kasamatsu, M. Tsubota, and M. Ueda, Vortices in multicomponent Bose-Einstein condensates, Int. J. Mod. Phys. B **19**, 1835 (2005).
[5] V. Schweikhard, I. Coddington, P. Engels, S. Tung, and E. A. Cornell, Vortex-Lattice Dynamics in Rotating Spinor Bose-Einstein Condensates, Phys. Rev. Lett. **93**, 210403 (2004).
[6] E. J. Mueller and T.-L. Ho, Two-Component Bose-Einstein Condensates with a Large Number of Vortices, Phys. Rev. Lett. **88**, 180403 (2002).
[7] K. Kasamatsu, M. Tsubota, and M. Ueda, Vortex Phase Diagram in Rotating Two-Component Bose-Einstein Condensates, Phys. Rev. Lett. **91**, 150406 (2003).
[8] R. Barnett, G. Refael, M. A. Porter, and H. P. Buchler, Vortex lattice locking in rotating two-component Bose-Einstein condensates, New J. Phys. **10**, 043030 (2008).
[9] P. Mason and A. Aftalion, Classification of the ground states and topological defects in a rotating two-component Bose-Einstein condensate, Phys. Rev. A **84**, 033611 (2011).
[10] C.-H. Hsueh, T.-L. Horng, S.-C. Gou, and W. C. Wu, Equilibrium vortex formation in ultrarapidly rotating two-component Bose-Einstein condensates, Phys. Rev. A **84**, 023610 (2011).
[11] R. Wei and E. Mueller, Vortex structures of a two-component Bose-Einstein condensate for large anisotropies, Phys. Rev. A **84**, 063611 (2011).
[12] A. Aftalion, P. Mason, and J. Wei, Vortex-peak interaction and lattice shape in rotating two-component Bose-Einstein condensates, Phys. Rev. A **85**, 033614 (2012).
[13] P. Kuopanportti, J. A. M. Huhtamäki, and M. Möttönen, Exotic vortex lattices in two-species Bose-Einstein condensates, Phys. Rev. A **85**, 043613 (2012).
[14] M. Cipriani and M. Nitta, Crossover between Integer and Fractional Vortex Lattices in Coherently Coupled Two-Component Bose-Einstein Condensates, Phys. Rev. Lett. **111**, 170401 (2013).
[15] N. Ghazanfari, A. Keleş, and M. Ö. Oktel, Vortex lattices in dipolar two-component Bose-Einstein condensates, Phys. Rev. A **89**, 025601 (2014).
[16] R. K. Kumar, L. Tomio, B. A. Malomed, and A. Gammal, Vortex lattices in binary Bose-Einstein condensates with dipole-dipole interactions, Phys. Rev. A **96**, 063624 (2017).
[17] B. M. Uranga and A. Lamacraft, Infinite lattices of vortex molecules in Rabi coupled condensates, Phys. Rev. A **97**, 043609 (2018).
[18] G. Thalhammer, G. Barontini, L. De Sarlo, J. Catani, F. Minardi, and M. Inguscio, Double Species Bose-Einstein Condensate with Tunable Interspecies Interactions, Phys. Rev. Lett. **100**, 210402 (2008).
[19] S. B. Papp, J. M. Pino, and C. E. Wieman, Tunable Miscibility in a Dual-Species Bose-Einstein Condensate, Phys. Rev. Lett. **101**, 040402 (2008).
[20] K. Kasamatsu and M. Tsubota, Vortex sheet in rotating two-component Bose-Einstein condensates, Phys. Rev. A **79**, 023606 (2009).
[21] P. N. Galteland, E. Babaev, and A. Sudbø, Fluctuation effects in rotating Bose-Einstein condensates with broken SU(2)

and U(1) × U(1) symmetries in the presence of intercomponent density-density interactions, Phys. Rev. A **91**, 013605 (2015).

[22] D. S. Hall, M. R. Matthews, J. R. Ensher, C. E. Wieman, and E. A. Cornell, Dynamics of Component Separation in a Binary Mixture of Bose-Einstein Condensates, Phys. Rev. Lett. **81**, 1539 (1998).

[23] E. J. Mueller, Spin textures in slowly rotating Bose-Einstein condensates, Phys. Rev. A **69**, 033606 (2004).

[24] M. Tylutki, L. P. Pitaevskii, A. Recati, and S. Stringari, Confinement and precession of vortex pairs in coherently coupled Bose-Einstein condensates, Phys. Rev. A **93**, 043623 (2016).

[25] L. A. Toikka, Vortex force in compressible spin-orbit-coupled Bose-Einstein condensates, Phys. Rev. A **96**, 033611 (2017).